INTEGRATIVE PHYSIOLOGY

Glycinergic interneurons are functionally integrated into the inspiratory network of mouse medullary slices

Stefan M. Winter · Jens Fresemann ·
Christian Schnell · Yoshitaka Oku ·
Johannes Hirrlinger · Swen Hülsmann

Abstract Neuronal activity in the respiratory network is functionally dependent on inhibitory synaptic transmission. Using two-photon excitation microscopy, we analyzed the integration of glycinergic neurons in the isolated inspiratory pre-Bötzinger complex-driven network of the rhythmic slice preparation. Inspiratory (96%) and 'tonic' expiratory neurons (4%) were identified via an increase or decrease, respectively, of the cytosolic free calcium concentration during the inspiratory-related respiratory burst. Furthermore, in BAC-transgenic mice expressing EGFP under the control of the GlyT2-promoter, 50% of calcium-imaged inspiratory neurons were glycinergic. Inspiratory bursting of glycinergic neurons in the slice was confirmed by whole-cell recording. We also found glycinergic neurons that receive phasic inhibition from other glycinergic neurons. Our calcium imaging data show that glycinergic neurons comprise a large population of inspiratory neurons in the pre-Bötzinger complex-driven network of the rhythmic slice preparation.

Keywords Glycine · Inhibitory synaptic transmission · Respiratory neurons · Imaging · Whole-cell recording

SMW, JF, and CS contributed equally.

Electronic supplementary material The online version of this article (doi:10.1007/s00424-009-0647-1) contains supplementary material, which is available to authorized users.

S. M. Winter · J. Fresemann · C. Schnell · S. Hülsmann (✉)
Abt. Neuro- und Sinnesphysiologie,
Zentrum Physiologie und Pathophysiologie,
Georg-August-Universität, Humboldtallee 23,
37073 Göttingen, Germany
e-mail: shuelsm2@uni-goettingen.de

S. M. Winter · J. Fresemann · C. Schnell · J. Hirrlinger ·
S. Hülsmann
DFG Forschungszentrum für Molekularphysiologie des Gehirns,
Göttingen, Germany

Y. Oku
Department of Physiology,
Hyogo College of Medicine,
Nishinomiya, Japan

Present address:
J. Hirrlinger
Interdisziplinäres Zentrum für klinische Forschung (IZKF),
Universität Leipzig, Inselstr. 22,
04103 Leipzig, Germany

Introduction

In adult mammals, glycinergic neurotransmission is thought to be vital for rhythmogenic medullary respiratory processes [27–29], whereas its relevance, e.g., for inspiratory phase termination, may be much less pronounced in newborns [12, 23]. However, the persistence of respiratory rhythm after blockade of glycinergic inhibition does not preclude conditional modulation of the respiratory network by glycine. For example, the loss of glial glycine uptake results in glycine-mediated depression of the network and early postnatal death [7].

The pre-Bötzinger complex (preBötC) in the lower brainstem is a brain area that appears to be capable of generating inspiratory-related activity [4, 5, 36, 38]. While glycinergic neurons seem to be located in the area of the preBötC [40], their role in inspiratory network function in the isolated preBötC is not clear. In the rhythmic slice preparation, phasic glycinergic inhibition of tonically spiking neurons during the inspiratory phase has been demonstrated [33]. Thus, it can be concluded that some inspiratory neurons are glycinergic and inhibit expiratory neurons during the inspiratory phase.

In this investigation, we studied the interaction of glycinergic neurons within the preBötC-driven network using two-photon excitation microscopy, whole-cell electrophysiological recording, and bacterial artificial chromosome (BAC) transgenic mice expressing enhanced green fluorescent protein (EGFP) under the control of the promoter for the neuronal glycine transporter type 2 (GlyT2) [34, 43]. We found that glycinergic neurons are inspiratory modulated and receive inspiratory-related glycinergic inputs. We suggest that these glycinergic inspiratory neurons comprise a major constituent of the (rhythmogenic) inspiratory network.

Materials and methods

Experimental animals

Wild-type mice and transgenic BAC(GlyT2-EGFP) mice expressing the green fluorescent protein EGFP in glycinergic neurons [43] were bred in the animal facility of the University Hospital Göttingen and treated in accordance with the guidelines of the German Physiological Society as well as the regulations of the State of Lower Saxony and the Federal Republic of Germany. Both wild-type mice and transgenic BAC(GlyT2-EGFP) mice were used for two-photon excitation microscopy in slices, while only BAC (GlyT2-EGFP) mice were used for whole-cell recordings and immunohistochemistry.

Preparation of respiratory slices containing the pre-Bötzinger complex

The preparation of living acute slices ("rhythmic slice preparation") has been described previously [7, 11, 24, 36]. In brief, mice at postnatal day 4–9 (P4–P9) were rapidly decapitated and the brain was removed. The brainstem was isolated in ice-cold saline and mounted on an agar block and transferred to a vibratome (VT1000S, Leica, Bensheim, Germany). Transverse slices were sectioned in a rostrocaudal direction using ~200-µm steps until the lower brainstem was reached and the inferior olive was visible. Then, a 600–650-µm-thick slice containing the preBötC was prepared. Using this procedure, the rhythmic population of neurons was found within the rostral part of the slice. This slice was transferred to the recording chamber, with the rostral side on top, to be continuously superfused with an oxygenated (95% O_2 and 5% CO_2) artificial cerebrospinal fluid containing (mM) 118 NaCl, 3 KCl, 1.5 $CaCl_2$, 1 $MgCl_2$, 1 NaH_2PO_4, 25 $NaHCO_3$, and 30 D-glucose (~330 mosM/l; pH 7.4). Temperature was slowly raised to 30°C. For long-term rhythmic activity, potassium concentration was increased to 8 mM.

Electrophysiology

To identify EGFP-fluorescent glycinergic neurons for electrophysiological analysis, slices were illuminated with a monochromator (excitation 467 nm; Polychrome II, TILL Photonics, Gräfelfing Germany), fiber-coupled to an upright microscope (Axioscope FS, Zeiss, Oberkochen, Germany) equipped with changeable filter sets (dichroic mirror 505 nm, band pass emission filter 545/50 nm). To optimize cell visibility for patch clamping, epifluorescence illumination was combined with infrared light illumination using a gradient contrast [3] and a CCD camera (Vx45, Optronics; Goleta, CA, USA, or Sensicam QE, PCO, Kehlheim, Germany). Images of fluorescent cells were captured and stored on a personal computer using ImagingWorkbench software (Indec BioSystems, Santa Clara, CA, USA).

Whole-cell recordings were performed with a Multiclamp 700A (Axon Instruments, Inc., Foster City, CA, USA) or an L/M-PCA patch clamp amplifier (E.S.F, Friedland, Germany). Recording electrodes were prepared from borosilicate capillaries (Biomedical Instruments, Zöllnitz, Germany) using a horizontal, programmable puller (Zeitz-Instrumente, Munich, Germany). Patch pipettes were filled with an intracellular solution containing (mM) 140 potassium gluconate, 1 $CaCl_2$, 2 $MgCl_2$, 4 Na_2ATP, 10 HEPES, 10 EGTA (pH, 7.2 (adjusted with KOH)) leading to a resistance between 3 and 6 MΩ. The calculated equilibrium potential $E_{[Cl]}$ for chloride was −87 mV.

Inspiratory-related field potentials were recorded in the ventrolateral area of the slice that contained the ventral respiratory column including the preBötC. Field potentials were recorded with custom-made, thick-walled single-barreled microelectrodes (~1 MΩ, 50–100 µm outer diameter) that were placed either ipsilateral or contralateral to the site of imaging or whole-cell recordings.

Neuronal population activity was amplified by a custom-built AC amplifier (5,000–10,000 times), band-pass-filtered (0.25–1.5 kHz), rectified, and integrated (Paynter filter; time constant 40–70 ms). Recordings were digitized at 10 kHz and stored using Axograph software (Axon Instruments, Inc., Foster City, CA, USA) or Chart software (ADInstruments Pty. Ltd., Mountain View, CA, USA).

Calcium imaging using two-photon excitation microscopy

Calcium imaging in the ventral respiratory column was performed with a custom-made two-photon microscope that is based on a commercial scan head (TriMScope, LaVision BioTec, Bielefeld, Germany). In this scan head, the pulsed infrared-laser beam can be divided into a line of up to 64 foci, increasing the amount of emitted light per time without increase of photo damage [21]. The scan head

was coupled to a fixed-stage, upright microscope (Axioscope FS2, Zeiss, Oberkochen, Germany), using ×40 (0.8 NA) or ×63 (1.0 NA) water immersion objectives (Zeiss, Oberkochen, Germany). Two-photon excitation was achieved by a titanium sapphire laser equipped with broadband optics (MaiTai BB, Spectra Physics, Darmstadt, Germany). For field detection of emitted light, we used CCD cameras (Ixon 885 Andor Technology, Belfast, Northern Ireland, or PCO; Sensicam QE; Kehlheim, Germany). Fast calcium imaging was performed using the multi-beam mode (16 or 32 beams) with scan fields of $200\times200\,\mu m$ (Ixon camera) or $170\times220\,\mu m$ (Sensicam QE). Exposure time was 25–40 ms (4×4 binning$=255\times256$ pixel) leading to sampling rates of 10 to 30 Hz. For higher spatial resolution, the number of beams was increased to 64 and images were taken with no binning at longer integration times. Laser power was controlled by a $\lambda/2$ plate and a sheet polarizer in the scan head, controlled by "ImSpector" imaging software (LaVision BioTec, Bielefeld, Germany), and 3D-Stacks with $10\,\mu m$ per step were taken using a piezo-focus (Physik Instrumente, Karlsruhe, Germany) to determine the spatial distribution of the respiratory neurons up to a depth of $100\,\mu m$. Deeper in the tissue, identification of cell borders was not possible. The microscope was also equipped with two photomultipliers (Hamamatsu Photonics, Hamamatsu, Japan) for non-descanned fluorescence detection. Non-descanned detection was used for high-resolution scanning together with $1\,\mu m$ z-stacks (Fig. 2).

Cell loading for calcium imaging

Multi-cell bolus loading was performed as described in detail earlier [37]. Briefly, $50\,\mu g$ Oregon green BAPTA-1AM (OGB-1-AM, Molecular Probes, Eugene, OR, USA) was dissolved in dimethyl sulfoxide ($5\,\mu l$) containing 20% Pluronic F-127 (Molecular Probes, Karlsruhe, Germany) and stored at $-20°C$ in 0.5-μl aliquots until used. For injection, one aliquot of this stock solution was dissolved in 5–$7\,\mu l$ of an extracellular solution containing (mM) 150 NaCl, 2.5 KCl, and 10 HEPES (pH adjusted to 7.4). The final concentration of OGB-1-AM was between 0.6 and 0.8 mM. A small amount of the solution was injected (2 bar; 2 min) 50–$100\,\mu m$ below the slice surface into the preBötC region using a patch pipette [44]. After injection, an incubation period of 30 min was allowed for sufficient dye loading.

Identification of EGFP-labeled neurons for calcium imaging

Calcium-signals in GlyT2-EGFP expressing neurons were analyzed using OGB-1-AM. The following method was adapted from Wilson and colleagues [41]. To determine the optimal parameters for discrimination of EGFP and OGB-1-

AM fluorescence, baseline fluorescence of six individual neurons stained with either of the fluorophores was determined for CFP (480/30 BP) and YFP (525/50 BP) emission filters, respectively, while the excitation wavelength of the laser was tuned from 780 to 920 nm (10-nm steps) (Supplemental Fig. 2). Similar results were obtained with the 511–551-nm (OGB-1-AM) and 450–500-nm (EGFP) band pass filters, respectively, which were used for the multi-beam mode. From these experiments, we concluded that changes of OGB-1-AM fluorescence can be faithfully detected at 800-nm excitation wavelength through a YFP-Filter, whereas EGFP-fluorescence was specifically detected at 900-nm excitation wavelength through the CFP filter. Optical filters were obtained from AHF Analysentechnik AG (Tübingen, Germany).

Immunohistochemistry

For choline acetyltransferase (ChAT) immunohistochemistry, adult mice (BAC(GlyT2-EGFP) mice, $n=3$) were deeply anesthetized with diethyl ether. Depth of anesthesia was confirmed by the absence of nociceptive reflexes. Animals were then cardio-perfused with Hanks' balanced salt solution followed by 4% paraformaldehyde in phosphate-buffered saline (PBS) as described before [42]. The brain was removed and placed for 24 h in the same fixative and stored thereafter in PBS with 0.01% sodium azide. Transverse or sagittal slices (50–$100\,\mu m$) were cut using a vibratome (VT1000S, Leica, Bensheim, Germany). Slices were permeabilized in 0.4% Triton in PBS for 30 min, and non-specific antibody binding was minimized by adding 4% normal donkey serum in PBS with 0.2% Triton. Sections were incubated with the primary anti-ChAT-antibody (Chemicon, Temecula, CA, USA) overnight in 1% serum in PBS with 0.05% Triton ($4°C$) and labeled with Cy5-conjugated secondary antibodies the following day (room temperature, 2 h, anti-goat from donkey, 1:250 dilution; Jackson IR, Newmarket, UK).

Fluorescence microscopy of immunostained brainstem sections was performed using a confocal laser scanning microscope (LSM 510 Meta, Zeiss, Oberkochen, Germany). EGFP was excited at 488 nm (argon laser). Fluorescence was detected through a 505–530-nm band pass filter. Cy5-fluorescence of secondary antibodies was visualized at 633 nm excitation (HeNe laser) through a 650-nm-long pass filter. Tile scans (for overview) were acquired using a motorized x-y table attached to the confocal microscope and multi-time series software extension (Zeiss, Oberkochen, Germany).

Data analysis

The two-photon excitation microscope was controlled by ImSpector imaging software (LaVision BioTec, Bielefeld,

Germany). For offline analyses, images were exported to TIFF format and processed with ImageJ software (http://rsb.info.nih.gov/ij/) using public macro routines provided by the Wright Cell Imaging Facility (http://www.uhnres.utoronto.ca/facilities/wcif/download.php). To correlate field potential recordings with optical signals, trigger pulses (TTL) for each image were recorded simultaneously with the field potential.

To perform cycle-triggered averaging, we developed a MATLAB (Mathworks Inc., Natick, MA, USA) routine. Optical signals from consecutive respiratory cycles were processed as follows. First, linear trends were removed, and signals were spatially averaged by 3×3 pixels. Then, a 20×20-pixels region of interest (ROI) was set on a strongly stained inspiratory neuron. Optical signals within the ROI were moving-time averaged (bin width=5 images) and high-pass filtered (time constant=50 images) to detect peaks of calcium transients associated with inspiratory activity. Using the frame position of inspiratory peaks as the reference, optical signals of 50 preceding and 100 following frames were averaged five to 20 times. Additionally, the cross-correlations between each pixel and the ROI were calculated.

Calcium changes were calculated as relative changes ($\Delta F/F_0$) from the averaged intensity of a ROI drawn with the "multi-measure" ROI macro of ImageJ. For quantitative analyses of glycinergic (EGFP-positive) neurons using two-photon imaging, we counted (a) the number of inspiratory glycinergic neurons, (b) the total number of glycinergic neurons, and (c) the total number of inspiratory neurons from five experiments using at least three (3–7) consecutive recordings at different depths of the slice (10 µm z-distance). A prerequisite for a recording to be analyzed was the identification of at least one respiratory neuron in the respective optical plane.

Quantification of inhibitory postsynaptic currents (IPSCs) was performed with MiniAnalysis program (Jaejin Software, Leonia, NJ, USA) using threshold-based event detection. The IPSC frequency was averaged from the reciprocal value of the inter-event interval.

Data were further analyzed with IGOR Pro (Wave-Metrics, OR, USA) and SigmaPlot/SigmaStat (Systat Software Inc., San Jose, CA, USA). Student's t tests were used to determine the significance of changes of IPSC amplitude and frequency. Results were expressed as mean± SEM and differences were considered significant if $P < 0.05$.

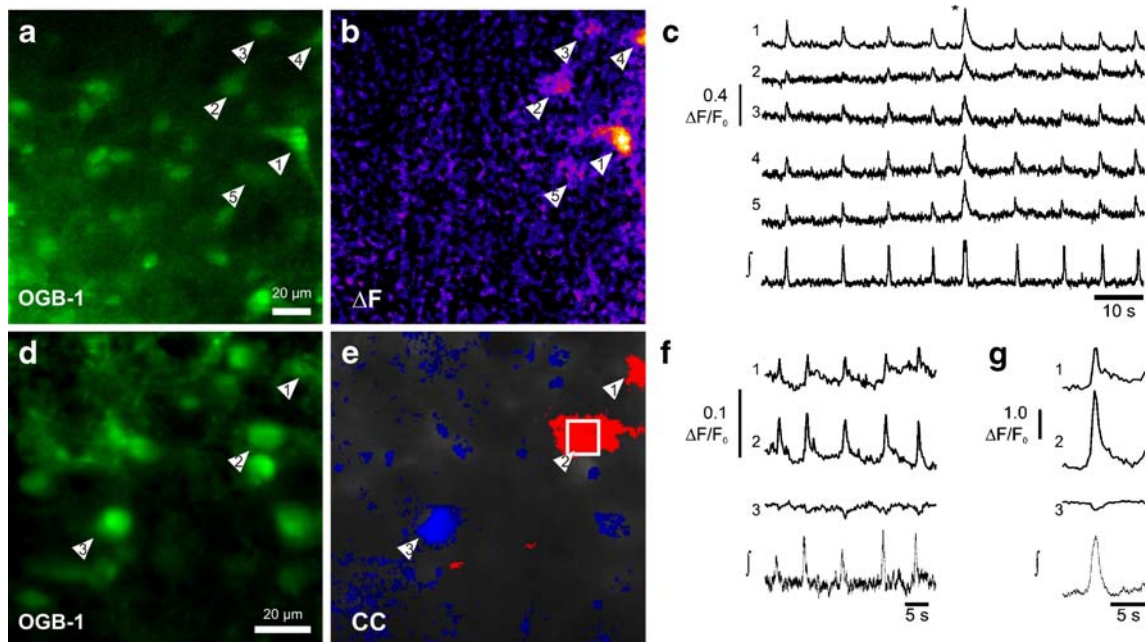Fig. 1 Two-photon excitation microscopy of respiratory neurons in the rhythmic slice preparation. a Oregon green BAPTA1-AM (OGB-1-AM) labeling of neurons located in the ventral respiratory column visualized by multi-focal two-photon excitation microscopy. b Calcium signal during a larger respiratory burst: ΔF image taken at the time marked by the *asterisk* in c showing changes (*orange*) of calcium concentration in five neurons (*arrowheads*). c Simultaneous recording of the population field potential (∫) and intracellular free cytosolic calcium transients. Traces in c show calcium changes (ΔF/ F_0) recorded from five respiratory neurons (*arrowheads* in a, b). d OGB-1-AM labeling of respiratory neurons. e Pseudo-color mapping of the cross-correlations (*CC*) of the calcium signals of inspiratory neurons. *Red color* indicates inspiratory neurons (CC>0.8) and *blue* indicates the inspiratory inhibition of an expiratory neuron (CC<−0.3). f The traces of calcium changes ($\Delta F/F_0$) of three neurons indicated in d and e depicted together with the simultaneous recording of the field potential (∫). g Same data as in f derived from cycle-triggered averaging of ten consecutive respiratory bursts

Results

Two-photon excitation microscopy of rhythmic neurons in the preBötC-driven network

In a first series of experiments, we performed field potential recordings and simultaneously imaged changes of the free intracellular calcium concentration in the ventral respiratory column in different depths of the rhythmic slice preparation (up to 100 μm within the slice, $n=36$ recordings from 12 slices). Cells showing rhythmic calcium transients in phase with the respiratory bursts were identified (Fig. 1). However, their number was variable. In a single optical section (200×200 μm), we found one to seven inspiratory neurons (3.4 ± 0.04; 36 optical sections). To exclude the possibility that neurons with small rhythmic calcium transients were missed, we performed cycle-triggered averaging to extract them, if present, from background fluorescence (Fig. 1g). After averaging, there was a small, but insignificant increase in the number of inspiratory neurons detected (3.9 ± 0.05 inspiratory neurons; 36 optical sections). To obtain a rough estimate of the number of inspiratory neurons we can reach with our imaging technique, we recorded stacks of optical sections ($\sim 200 \times 200$ μm) at 10-μm intervals of distance between slice surface and a depth of 100 μm in the tissue. In this volume, the average number of imaged inspiratory neurons was 20.0 ± 4.5 ($n=6$ slices).

In three rhythmic slices, we observed inspiratory-related calcium signals that were larger than preceding and subsequent signals (Fig. 1c). Synchronous calcium signals could be observed in almost all inspiratory neurons of the particular focal plane. These larger calcium signals were each correlated with a larger burst in the field potential, which was followed by a relatively longer post-inspiratory pause. Field potential changes of similar shape and amplitude have been hypothesized to represent the electrophysiological correlate of sighs [18].

Calcium imaging of putative expiratory neurons

In the electrophysiological analysis of rhythmic slices, tonically active neurons, which are inhibited during inspiratory bursts, have been considered to be expiratory neurons [24, 33]. Such a behavior of neurons should result in a reduction of fluorescence of the calcium indicator dye during inspiration. Indeed, we were able to confirm the existence of such patterns (Fig. 1d–g), however, only in five cells in four slices.

Since the number of expiratory neurons was very low, we tested whether the duration of inspiratory inhibition of these cells is too short for a decay of the fluorescent signal. We performed calcium imaging in whole-cell-recorded neurons loaded with OGB-1, which showed tonic spike discharges. Hyperpolarization of the cell for a period of 1 s, 0.5 s, and 0.25 s, respectively, revealed a decrease in fluorescence of variable amplitude ($n=4$; Supplementary Fig. 1). A shorter hyperpolarization (0.125 and 0.063 s, respectively) never resulted in a decrease of fluorescence ($n=4$; Supplementary Fig. 1).

Identification of glycinergic neurons

The previous data imply that both inspiratory and tonic "expiratory" neurons are colocalized in the inspiratory network of the slice preparation and that tonic "expiratory" neurons receive synaptic inhibition during inspiratory activity. Thus, in the next step, we attempted to determine whether glycinergic neurons are responsible for this phasic inhibition. Glycinergic neurons are considered key elements of the primary oscillator in the respiratory network in vivo [25]. To test their contribution to rhythmicity in vitro in the ventral respiratory column of the neonatal mouse, we used EGFP-labeled glycinergic neurons [43]. In transverse sections of the medulla, EGFP fluorescence was strong throughout the slice (Fig. 2). Regions that showed strong expression of ChAT, such as the nucleus ambiguus, lacked cell bodies of glycinergic neurons (Fig. 2a–f). The shapes of glycinergic neurons labeled with EGFP were variable, including both fusiform and multi-polar (Fig. 2g; see Supplemental Movie).

Glycinergic neurons show inspiratory calcium transients

Two-photon excitation microscopy was used to test whether EGFP-positive glycinergic neurons are active during the inspiratory phase of the rhythm (Fig. 3a; see "Materials and Methods" and Supplementary Figs. 2 and 3 for details of separation of EGFP and OGB-1-AM fluorescence).

As hypothesized, inspiratory activity could be detected as calcium transients in EGFP-labeled neurons (Fig. 3b, c). About 50% (35 of 70 neurons; $n=5$ slices) of inspiratory neurons were glycinergic, as revealed by EGFP expression. Calcium transients accompanied inspiratory phase discharges in about 20% of the glycinergic neurons (35 of 176 EGFP-labeled neurons tested in five slices; Fig. 3d). Thus, glycinergic neurons represent a major subgroup of inspiratory cells in the ventral respiratory column of the neonatal rhythmic slice preparation.

Glycinergic neurons receive excitatory and inhibitory input during inspiration

To further analyze the integration of glycinergic neurons in the preBötC-driven network, we conducted whole-cell current clamp recordings from EGFP-labeled cells.
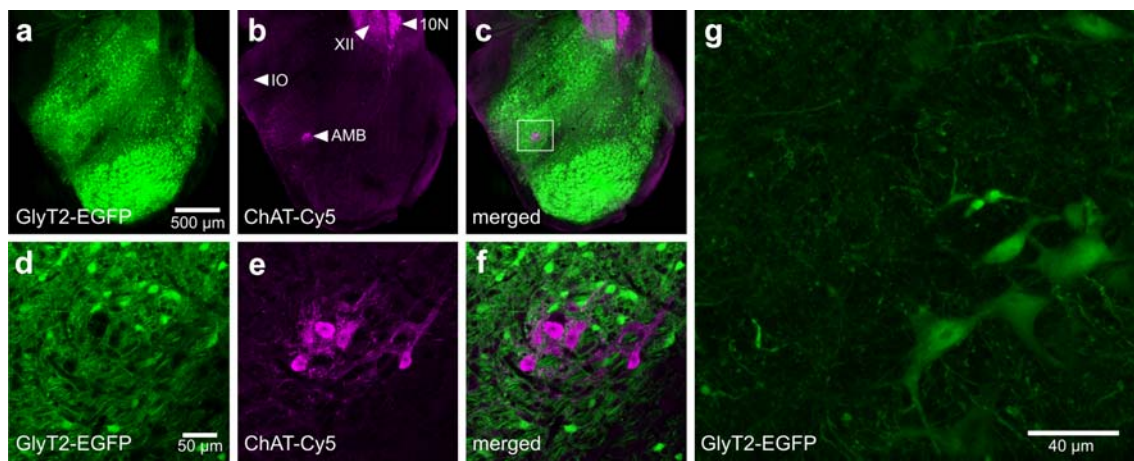
Fig. 2 Distribution of EGFP-labeled glycinergic neurons in the caudal medulla. **a–c** Overview of the distribution of EGFP-labeled glycinergic neurons in BAC(GlyT2-EGFP)-mice (**a**) and the expression of the choline acetyltransferase (*ChAT*) (**b**) in the caudal medulla. ChAT-antibody was detected by Cy5-conjugated fluorescent secondary antibodies and visualized by confocal laser scanning microscopy. The overlay of both channels is shown in **c**. **d–f** Magnification of the region of the nucleus ambiguus identified by high levels of ChAT expression (**e**). No glycinergic neurons are found in the pars compacta of the nucleus ambiguus. **f** Overlay of **d** and **e** reveals no EGFP expression in ChAT-positive neurons. *XII* hypoglossal nucleus, *IO* inferior olive, *10N* dorsal motor nucleus of vagus, *AMB* nucleus ambiguus. **g** This panel shows the morphology of glycinergic neurons. The maximum intensity projection of 82 images from a stack of two-photon excitation microscopy scans is shown (1 μm per step)

Approximately, 50% of the glycinergic neurons showed a tonic firing pattern (28/54 glycinergic neurons; Fig. 4a, b). Consistent with our two-photon imaging data, we found glycinergic neurons that received excitatory synaptic inputs in phase with the preBötC-driven field potential burst ($n=8$; Fig. 4c–e). These excitatory inputs were capable to produce a phasic increase of action potential frequency in four glycinergic neurons (Fig. 4d). Injection of steady hyperpolarizing current resulted in periodic bursts of action potentials that were in synchrony with the field potential (Fig. 4e). One labeled glycinergic neuron, by contrast, exhibited periodic inhibition of discharge that was time-locked to the population field potential.

Glycinergic neurons receive phasic glycinergic inputs

We then tested whether glycinergic neurons receive inhibitory inputs from other inhibitory neurons activated during the inspiratory phase. To discriminate IPSCs from excitatory postsynaptic currents, we clamped the EGFP-labeled glycinergic neurons to different holding potentials using patch pipettes with a low intracellular chloride concentration (equilibrium potential $E_{(Cl^-)}$ −87 mV). At a holding potential of −70 mV, a rhythmic increase of inward currents in phase with preBötC-driven field potential bursts was recorded, confirming that glycinergic neurons receive inspiratory input ($n=18$; Fig. 5b). Since the $E_{(Cl^-)}$ was −87 mV, phasic postsynaptic inward currents at −70 mV holding potential can be considered excitatory. However, recordings at a holding potential of −50 or −40 mV increased chloride currents and revealed a phasic increase of both outward-going (inhibitory, chloride-mediated) and inward-going (excitatory) postsynaptic currents during inspiratory bursts (Fig. 5c, d). Furthermore, at a holding potential of 0 mV (Fig. 5e), which was close to the reversal potential for excitatory synaptic transmission, only outward currents were recorded in phase with inspiratory preBötC activity, indicating that glycinergic neurons also receive phasic synaptic inhibition from other respiratory neurons ($n=11$).

To quantify these phasic IPSCs, we compared the frequency and amplitude of IPSCs during the inspiratory burst with the preceding inter-burst interval. Under control conditions, we measured a 43.8 ± 8.0 increase of the IPSC frequency (53.1 ± 17.5 vs. 29.8 ± 10.0 Hz; $p<0.05$; $n=6$) and an $18.0\pm7.0\%$ (44.5 ± 9.6 vs. 34.2 ± 6.2 pA; $p<0.05$; $n=6$) increase of the IPSC amplitude during the respiratory burst. The averaged duration of this increase of IPSC frequency was 507 ± 54 ms, which corresponds to a duration of the integrated field potential of 524 ± 56 ms ($n=6$).

To test whether this phasic inhibition results from glycinergic neurons, we applied the glycine receptor antagonist strychnine. Application of 2 μM strychnine blocked most of the rhythmic outward current at 0 mV ($n=5$; Fig. 6). The phasic inspiratory increase of the IPSC amplitude was completely blocked (26.5 ± 3.8 pA during the burst and 26.2 ± 3.2 pA during the preceding interval). There was still a small increase of the IPSC frequency in two experiments. The average IPSC frequency from five experiments was 24.9 ± 9.3 Hz during the burst and $18.1\pm$
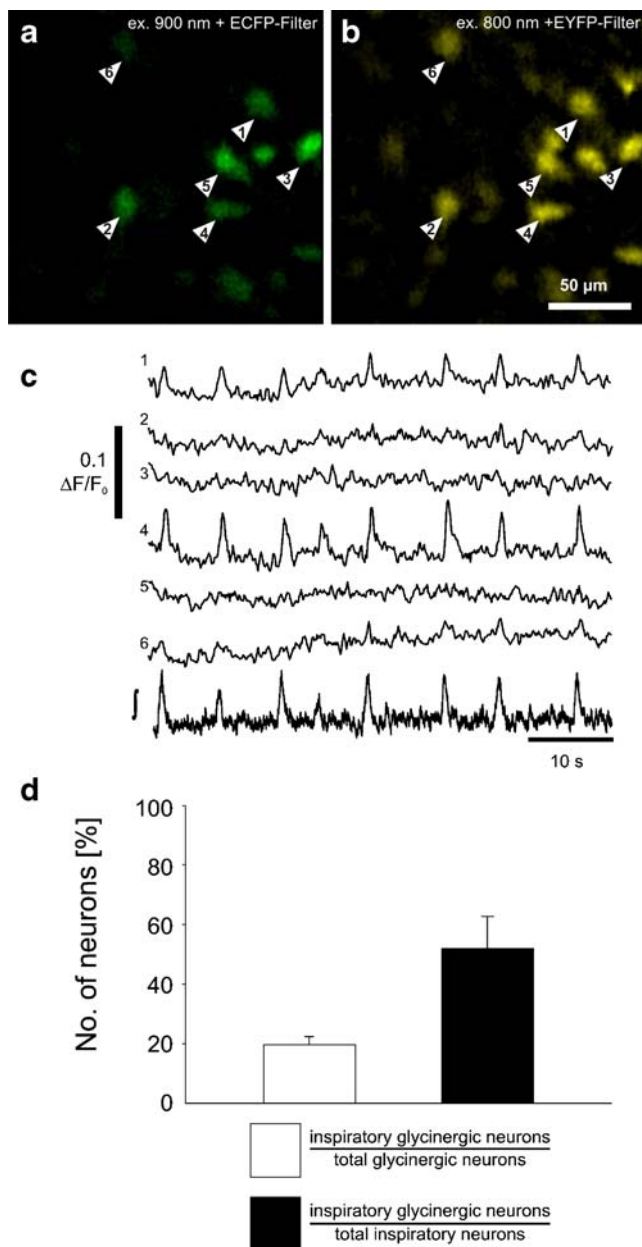
8.0 Hz during the preceding burst interval ($n=5$, n.s.). An additional increase of the strychnine concentration to 10 μM further reduced the outward current, both during the burst (15.2±6.2 pA) as well as in the inter-burst interval (15.0±6.6 pA; $n=5$). In two experiments, a small phasic IPSC frequency increase remained, indicating the presence of phasic GABAergic IPSCs. In one case, additional application of 5 μM bicuculline blocked the remaining rhythmic outward current (not shown).

Fig. 3 Rhythmic calcium transients in glycinergic neurons. **a** Identification of GlyT2-EGFP neurons (*arrowheads*) by two-photon excitation at 900 nm and CCD camera detection with a CFP optimized filter (465–495 nm). **b** OGB-1-AM fluorescence is shown and measured by using 800 nm excitation wavelength and a 501–551-nm emission band pass filter. All GlyT2-EGFP cells (**a**) appear to be labeled by OGB-1-AM (**b**). **c** Intracellular free cytosolic calcium transients recorded from glycinergic neurons. The numbering of the traces corresponds with the numbering of the neurons in the images **a** and **b**. The *lower trace* ($\int$) shows the integrated population field potential from the preBötC. **d** Graphic summary of the experiments. The *left bar* (*white*) shows the percentage of inspiratory EGFP-expressing glycinergic neurons (over the total number of glycinergic neurons). The *right bar* (*black*) shows the percentage of inspiratory glycinergic neurons (over the total number of inspiratory neurons). Data are given as mean±SEM based on 20 imaging planes from five slices
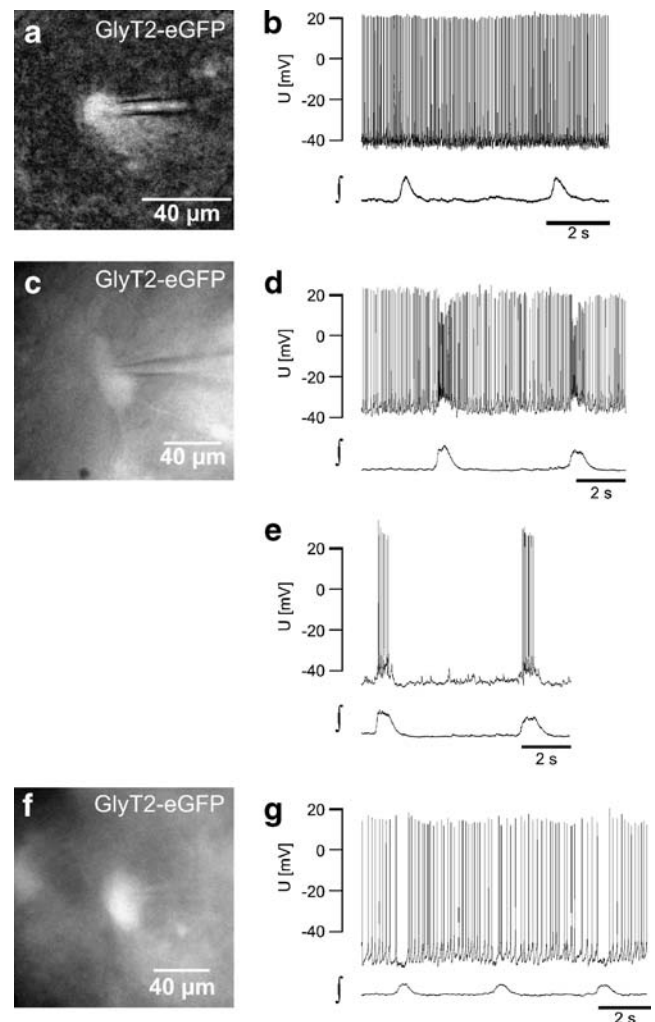
Fig. 4 **a** CCD camera image of the EGFP-expression of a glycinergic neuron recorded in **b** (epifluorescence, excitation using 467 nm). **b** Current clamp recording of the glycinergic neuron (in **a**) showing tonic spike activity without rhythmic modulation ($\int$ integral of the population field potential). **c–e** Example of a glycinergic neuron (**c**) that receives phasic excitatory input. **d** Current clamp recording showing tonic activity with a phasic increase of action potential frequency. **e** Injection of negative current (−40 pA) results in a cessation of tonic activity and uncovers bursts of action potentials resulting from phasic excitation. **f, g** Glycinergic neuron (**f**) showing a phasic reduction of action potential frequency, the typical behavior of a tonic expiratory neuron (**g**)
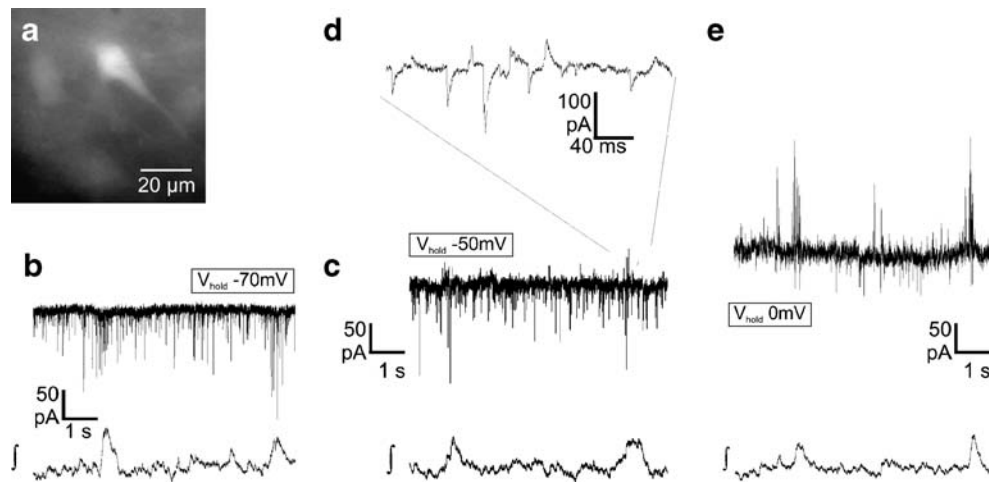
Fig. 5 Glycinergic neurons receive inhibitory and excitatory inputs simultaneously. **a–e** Whole-cell voltage-clamp recordings of a glycinergic neuron (**a**), which receives rhythmic both excitatory and inhibitory inputs in phase with rhythmic (integrated) network activity ($\int$). Holding potential was −70 mV (**b**), −50 mV (**c, d**), and 0 mV (**e**). The calculated equilibrium potential $\left(E_{(Cl^-)}\right)$ for chloride was −87 mV (see "Materials and methods"). Changing the holding potential to −50 mV (**c, d**) allowed discrimination of inward-going excitatory and outward-going inhibitory chloride-mediated postsynaptic currents, confirming that GlyT2-EGFP neurons rhythmically receive both excitatory and inhibitory inputs

Discussion

Functional two-photon excitation microscopy of respiratory neurons

We employed calcium imaging using two-photon excitation microscopy of respiratory neurons in the rhythmic slice preparation. This preparation includes the preBötC, which contains neurons essential for rhythmogenesis [24, 36].
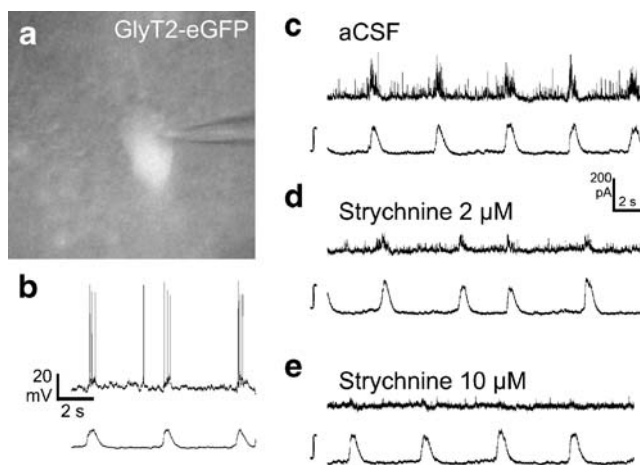

Fig. 6 Glycinergic neurons receive inspiratory-related glycinergic inhibition. **a, b** CCD camera image (**a**) and original traces from current clamp recording (**b**; holding current −100 pA) of an inspiratory glycinergic neuron from the ventral respiratory column. **c–e** Whole-cell voltage-clamp recordings at a holding potential of 0 mV. **c** The recording shows a phasic increase of the frequency and amplitude of inhibitory postsynaptic currents during the inspiratory burst. **d, e** Inhibition of glycine receptors by 2 μM (**d**) or 10 μM (**e**) strychnine strongly reduces the IPSC amplitude

Using the inferior olive as a landmark for sectioning, the preBötC is located close to the rostral surface of the rhythmic slice preparation, and respiratory neurons can be analyzed by electrophysiology or imaging [7, 11, 42, 44]. The rostro-caudal extension of the neuron population necessary for the generation of the respiratory rhythm in a slice might be less than 100 μm in neonatal rats [31]. Although such data are not available for neonatal mice, we cannot exclude the fact that some of the imaged neurons were located outside the preBötC [31].

Analysis of respiratory neurons within this slice preparation using calcium fluorescence imaging [6, 16, 44], confocal laser scanning microscopy [32], or two-photon excitation microscopy [9, 32] has been performed previously. Temporal resolution of conventional fluorescence imaging is sufficient, reaching 10 Hz or more [44], but z-axis resolution is limited due to off-focus fluorescence. This problem is solved by two-photon excitation microscopy [10], where the excitation process is limited to a small volume around the focal plane (although the resolution in the z-axis remains weaker than in the x- or y-axis [20]). However, one disadvantage of the point scanning technique is a lower temporal resolution [9, 32].

In this study, we combined the advantages of both techniques by using a microscope setup with a multi-focal scan head that splits the pulsed infrared laser beam into a line of up to 64 foci for excitation as well as a fast CCD camera for detection [21]. The scanning process was accelerated while maintaining the optical z-resolution inherent to two-photon excitation. The analysis of rhythmically active neurons was still confined to superficial layers (100 μm) of the slice near the rostral end of the preBötC and

hence the glycinergic neurons imaged included cells near the Bötzinger complex–preBötC border. The spatial distribution and relative numbers of rhythmically active glycinergic neurons in rostro-caudal extension of the preBötC network remain to be established.

Inspiratory glycinergic inhibition in the preBötC-driven network

Two-photon excitation microscopy revealed that ~50% of all OGB-1-AM-loaded inspiratory neurons in the preBötC-driven network were glycinergic (Fig. 3). The observation of such a high number of inspiratory glycinergic neurons supports the notion that phasic inhibition in the rhythmic slice preparation relies almost exclusively on glycinergic inhibition [24, 33]. We assume that the majority (~80%) of glycinergic neurons did not show any respiratory calcium signal, either because they were silent or because they are tonically discharging. This finding is in line with our whole-cell recording data, showing that 50% of the recorded glycinergic neurons were tonically discharging (Fig. 4). However, in a subset of glycinergic neurons that showed tonic inter-burst discharges, we observed a strong increase of action potential frequency during the respiratory bursts. Since two-photon excitation microscopy with OGB-1 can detect a rise of the free intracellular calcium activity resulting from two to three additional action potentials, some of the inspiratory calcium transients we recorded in glycinergic neurons might result from the latter type of neuron.

In our two-photon excitation microscopy experiments, inspiratory neurons clearly outnumbered expiratory neurons. A possible explanation of the low number of expiratory neurons could be a delayed time course of the developmental reversal of the chloride equilibrium potential ($E_{[Cl]}$) in tonic neurons, as compared to inspiratory neurons. In inspiratory neurons of mice [30], the $E_{[Cl]}$ reaches its final negative level approximately at postnatal day 4. If the $E_{[Cl]}$ in expiratory neurons remains slightly more depolarized during the second half of the first postnatal week, hyperpolarization would not occur, although shunting inhibition might be effective. The perinatal shift of the $E_{[Cl]}$ in the respiratory centers is, however, still a matter of debate. In contrast to mice, the $E_{[Cl]}$ in respiratory neurons of rats is negative to the resting potential at birth [1, 26]

While the issue of developmental $E_{[Cl]}$ changes requires further evaluation, we can exclude the possibility that OGB-1 is not sensitive enough to detect a decay of fluorescence during the inspiratory inhibition. An interruption of the discharge of spiking neurons, as little as 250 ms, can be detected by a decay of the OGB-1 fluorescence (Supplemental Fig. 1G, H). Although the duration of the phasic IPSC increase in glycinergic neurons lasts approx-

imately 500 ms, IPSCs from a single inspiratory glycinergic neuron may not be sufficient to generate an expiratory discharge pattern in the other neuron. Further efforts are necessary to determine how many inspiratory glycinergic neurons are necessary to sufficiently inhibit a tonic neuron.

Relevance of glycinergic inhibition in the preBötC-driven network

In the rhythmic slice preparation, glycinergic inhibition is less important than in the intact animal, since rhythmic neuronal activity persists after complete blockade of both GABAergic and glycinergic synaptic inhibition [12]. Nevertheless, disturbances of synaptic inhibition do affect the network activity of the slice: Although strychnine does not affect the rhythm in the slice early postnatally [7, 33], pharmacological blockade of glycinergic inhibition in slices from older animals (>P8) accelerates the respiratory rhythm [44]. This might be related to a change of the reversal potential of chloride to more negative values after postnatal day 4 [30]. The respiratory rhythm, which persists after blockade of glycine receptors in slice preparations from older animals, is quite labile since additional blockade of calcium-activated potassium channels (BK channels) results in a severe reduction of the preBötC-driven inspiratory activity in the slice preparation [44]. BK channels may comprise a compensatory mechanism that supports burst termination [44] and stabilizes rhythm in the slice preparation. Further experiments may determine whether phasic activity of glycinergic neurons contributes to burst termination in the presumed rhythm generating excitatory neuron population of the pre-Bötzinger complex [4].

Functional significance of inspiratory inhibitory neurons in the slice network

Glycinergic neurons are a functionally inhomogeneous cell population comprising tonic neurons and inspiratory and a few expiratory neurons (see Fig. 4). Additionally, EGFP-negative neurons were identified with two-photon excitation microscopy, which might be glutamatergic, and include some with intrinsic bursting properties [2, 14, 39]. Glutamatergic neurons conduct rhythm to pre-motoneurons located dorsally to nucleus ambiguus [15], outside the region that we imaged in this study. Some EGFP-negative inspiratory neurons might also be GABAergic [17]. Another population of EGFP-positive inspiratory neurons labeled in the transgenic mouse line could be GABAergic as well as glycinergic, because co-release of GABA and glycine from inhibitory neurons occurs in the spinal cord and brainstem [13, 19, 22, 35]. Since GlyT2 is a necessary transporter for filling synaptic vesicles with glycine [8], we can assume that every EGFP-labeled neuron releases

glycine. In addition to activation of silent glycinergic neurons, the excitatory input from inspiratory neurons can cause a phasic increase of discharge rate. Depending on the state of the overall excitatory input to a glycinergic neuron, its firing pattern might vary between bursting and tonically firing. We showed unequivocally that glycinergic neurons receive glycinergic inhibition. Although the functional importance remains to be determined, inspiratory glycinergic neurons might gain–modulate inspiratory drive in the rhythm-generating network.

Summary

In the rhythmic slice preparation of transgenic mice with cell-type-specific expression of fluorescent proteins and in combination with two-photon excitation microscopy of calcium indicator dyes, we demonstrated that glycinergic inhibition is functionally integrated into preBötC-driven network activity. We propose that local glycinergic inhibitory circuits make important contributions to the generation and maintenance of the respiratory rhythm.

References

1. Brockhaus J, Ballanyi K (1998) Synaptic inhibition in the isolated respiratory network of neonatal rats. Eur J Neurosci 10:3823–3839

2. Del Negro CA, Morgado-Valle C, Feldman JL (2002) Respiratory rhythm: an emergent network property? Neuron 34:821–830

3. Dodt H, Eder M, Frick A, Zieglgansberger W (1999) Precisely localized LTD in the neocortex revealed by infrared-guided laser stimulation. Science 286:110–113

4. Feldman JL, Del Negro CA (2006) Looking for inspiration: new perspectives on respiratory rhythm. Nat Rev Neurosci 7:232–242

5. Feldman JL, Janczewski WA (2006) The Last Word: Point: Counterpoint authors respond to commentaries on "the parafacial respiratory group (pFRG)/pre-Botzinger complex (preBotC) is the primary site of respiratory rhythm generation in the mammal". J Appl Physiol 101:689

6. Funke F, Dutschmann M, Müller M (2007) Imaging of respiratory-related population activity with single-cell resolution. Am J Physiol 292:C508–C516

7. Gomeza J, Hülsmann S, Ohno K, Eulenburg V, Szoke K, Richter D, Betz H (2003) Inactivation of the glycine transporter 1 gene

8. Gomeza J, Ohno K, Hülsmann S, Armsen W, Eulenburg V, Richter DW, Laube B, Betz H (2003) Deletion of the mouse glycine transporter 2 results in a hyperekplexia phenotype and postnatal lethality. Neuron 40:797–806

9. Hayes JA, Del Negro CA (2007) Neurokinin receptor-expressing pre-Botzinger complex neurons in neonatal mice studied in vitro. J Neurophysiol 97:4215–4224

10. Helmchen F, Denk W (2005) Deep tissue two-photon microscopy. Nat Methods 2:932–940

11. Hülsmann S, Oku Y, Zhang W, Richter DW (2000) Metabolic coupling between glia and neurons is necessary for maintaining respiratory activity in transverse medullary slices of neonatal mouse. Eur J Neurosci 12:856–862

12. Johnson SM, Koshiya N, Smith JC (2001) Isolation of the kernel for respiratory rhythm generation in a novel preparation: the pre-Botzinger complex "island". J Neurophysiol 85:1772–1776

13. Jonas P, Bischofberger J, Sandkuhler J (1998) Corelease of two fast neurotransmitters at a central synapse. Science 281:419–424

14. Koizumi H, Smith JC (2008) Persistent Na+and K+-dominated leak currents contribute to respiratory rhythm generation in the pre-Botzinger complex in vitro. J Neurosci 28:1773–1785

15. Koizumi H, Wilson CG, Wong S, Yamanishi T, Koshiya N, Smith JC (2008) Functional imaging, spatial reconstruction, and biophysical analysis of a respiratory motor circuit isolated in vitro. J Neurosci 28:2353–2365

16. Koshiya N, Smith JC (1999) Neuronal pacemaker for breathing visualized in vitro. Nature 400:360–363

17. Kuwana S, Tsunekawa N, Yanagawa Y, Okada Y, Kuribayashi J, Obata K (2006) Electrophysiological and morphological characteristics of GABAergic respiratory neurons in the mouse pre-Botzinger complex. Eur J Neurosci 23:667–674

18. Lieske SP, Thoby-Brisson M, Telgkamp P, Ramirez JM (2000) Reconfiguration of the neural network controlling multiple breathing patterns: eupnea, sighs and gasps [see comment]. Nat Neurosci 3:600–607

19. Muller E, Le Corronc H, Triller A, Legendre P (2006) Developmental dissociation of presynaptic inhibitory neurotransmitter and postsynaptic receptor clustering in the hypoglossal nucleus. Mol Cell Neurosci 32:254–273

20. Müller M, Schmidt J, Mironov SL, Richter DW (2003) Construction and performance of a custom-built two-photon laser scanning system. J Phys D Appl Phys 36:1747–1757

21. Niesner R, Andresen V, Neumann J, Spiecker H, Gunzer M (2007) The power of single and multibeam two-photon microscopy for high-resolution and high-speed deep tissue and intravital imaging. Biophys J 93:2519–2529

22. O'Brien JA, Berger AJ (1999) Cotransmission of GABA and glycine to brain stem motoneurons. J Neurophysiol 82:1638–1641

23. Paton JF, Richter DW (1995) Role of fast inhibitory synaptic mechanisms in respiratory rhythm generation in the maturing mouse. J Physiol 484:505–521

24. Ramirez JM, Quellmalz UJ, Richter DW (1996) Postnatal changes in the mammalian respiratory network as revealed by the transverse brainstem slice of mice. J Physiol 491(Pt 3):799–812

25. Ramirez JM, Telgkamp P, Elsen FP, Quellmalz UJ, Richter DW (1997) Respiratory rhythm generation in mammals: synaptic and membrane properties. Respir Physiol 110:71–85

26. Ren J, Greer JJ (2006) Modulation of respiratory rhythmogenesis by chloride-mediated conductances during the perinatal period. J Neurosci 26:3721–3730

27. Richter D (1996) Neural regulation of respiration: rhythmogenesis and afferent control. In: Gregor R, Windhorst U (eds) Comprehensive human physiology. Springer, Berlin

discloses vital role of glial glycine uptake in glycinergic inhibition. Neuron 40:785–796

28. Richter DW, Ballanyi K, Schwarzacher S (1992) Mechanisms of respiratory rhythm generation. Curr Opin Neurobiol 2:788–793

29. Richter DW, Spyer KM (2001) Studying rhythmogenesis of breathing: comparison of in vivo and in vitro models. Trends Neurosci 24:464–472

30. Ritter B, Zhang W (2000) Early postnatal maturation of GABAA-mediated inhibition in the brainstem respiratory rhythm-generating network of the mouse. Eur J Neurosci 12:2975–2984

31. Ruangkittisakul A, Schwarzacher SW, Secchia L, Ma Y, Bobocea N, Poon BY, Funk GD, Ballanyi K (2008) Generation of eupnea and sighs by a spatiochemically organized inspiratory network. J Neurosci 28:2447–2458

32. Ruangkittisakul A, Schwarzacher SW, Secchia L, Poon BY, Ma Y, Funk GD, Ballanyi K (2006) High sensitivity to neuromodulator-activated signaling pathways at physiological [K+] of confocally imaged respiratory center neurons in on-line-calibrated newborn rat brainstem slices. J Neurosci 26:11870–11880

33. Shao XM, Feldman JL (1997) Respiratory rhythm generation and synaptic inhibition of expiratory neurons in pre-Botzinger complex: differential roles of glycinergic and GABAergic neural transmission. J Neurophysiol 77:1853–1860

34. Simat M, Ambrosetti L, Lardi-Studler B, Fritschy JM (2007) GABAergic synaptogenesis marks the onset of differentiation of basket and stellate cells in mouse cerebellum. Eur J Neurosci 26:2239–2256

35. Singer JH, Berger AJ (2000) Development of inhibitory synaptic transmission to motoneurons. Brain Res Bull 53:553–560

36. Smith JC, Ellenberger HH, Ballanyi K, Richter DW, Feldman JL (1991) Pre-Botzinger complex: a brainstem region that may generate respiratory rhythm in mammals. Science 254:726–729

37. Stosiek C, Garaschuk O, Holthoff K, Konnerth A (2003) In vivo two-photon calcium imaging of neuronal networks. Proc Natl Acad Sci U S A 100:7319–7324

38. Tan W, Janczewski WA, Yang P, Shao XM, Callaway EM, Feldman JL (2008) Silencing preBotzinger complex somatostatin-expressing neurons induces persistent apnea in awake rat. Nat Neurosci 11:538–540

39. Thoby-Brisson M, Ramirez J-M (2001) Identification of two types of inspiratory pacemaker neurons in the isolated respiratory neural network of mice. J Neurophysiol 86:104–112

40. Wang H, Stornetta RL, Rosin DL, Guyenet PG (2001) Neurokinin-1 receptor-immunoreactive neurons of the ventral respiratory group in the rat. J Comp Neurol 434:128–146

41. Wilson JM, Dombeck DA, Diaz-Rios M, Harris-Warrick RM, Brownstone RM (2007) Two-photon calcium imaging of network activity in XFP-expressing neurons in the mouse. J Neurophysiol 97:3118–3125

42. Winter SM, Hirrlinger J, Kirchhoff F, Hülsmann S (2007) Transgenic expression of fluorescent proteins in respiratory neurons. Respir Physiol Neurobiol 159:108–114

43. Zeilhofer HU, Studler B, Arabadzisz D, Schweizer C, Ahmadi S, Layh B, Bosl MR, Fritschy JM (2005) Glycinergic neurons expressing enhanced green fluorescent protein in bacterial artificial chromosome transgenic mice. J Comp Neurol 482:123–141

44. Zhao MG, Hülsmann S, Winter SM, Dutschmann M, Richter DW (2006) Calcium-regulated potassium currents secure respiratory rhythm generation after loss of glycinergic inhibition. Eur J Neurosci 24:145–154